Journal of Biomechanics 45 (2012) 2899–2906

Contents lists available at SciVerse ScienceDirect

Journal of Biomechanics

journal homepage: www.elsevier.com/locate/jbiomech
www.JBiomech.com

Human head–neck computational model for assessing blast injury

J.C. Roberts [a,*], T.P. Harrigan [a], E.E. Ward [a], T.M. Taylor [a], M.S. Annett [b], A.C. Merkle [a]

[a] The Johns Hopkins University, Applied Physics Laboratory, 10020 Johns Hopkins Road, Laurel, MD 20723, USA
[b] NASA Langley Research Center, Hampton, VA 23681, USA

ARTICLE INFO

Article history:
Accepted 24 July 2012

Keywords:
Brain injury
Finite element models (FEM)
Surrogate models
Blast
Human models

ABSTRACT

A human head finite element model (HHFEM) was developed to study the effects of a blast to the head. To study both the kinetic and kinematic effects of a blast wave, the HHFEM was attached to a finite element model of a Hybrid III ATD neck. A physical human head surrogate model (HSHM) was developed from solid model files of the HHFEM, which was then attached to a physical Hybrid III ATD neck and exposed to shock tube overpressures. This allowed direct comparison between the HSHM and HHFEM. To develop the temporal and spatial pressures on the HHFEM that would simulate loading to the HSHM, a computational fluid dynamics (CFD) model of the HHFEM in front of a shock tube was generated. CFD simulations were made using loads equivalent to those seen in experimental studies of the HSHM for shock tube driver pressures of 517, 690 and 862 kPa. Using the selected brain material properties, the peak intracranial pressures, temporal and spatial histories of relative brain–skull displacements and the peak relative brain–skull displacements in the brain of the HHFEM compared favorably with results from the HSHM. The HSHM sensors measured the rotations of local areas of the brain as well as displacements, and the rotations of the sensors in the sagittal plane of the HSHM were, in general, correctly predicted from the HHFEM. Peak intracranial pressures were between 70 and 120 kPa, while the peak relative brain–skull displacements were between 0.5 and 3.0 mm.

1. Introduction

A number of finite element model (FEM) of the human have been developed to model intracranial pressures, relative brain–skull displacements and stresses and strains within the brain in order to predict injury due to blunt trauma; Ruan et al. (1993), Claessens et al. (1997), Brands (2002), Kang et al. (1997), Kleiven (2002), Horgan and Gilchrist (2003) and Takhounts et al. (2003). These models were used to perform accident reconstruction studies (Willinger and Baumgartner, 2003; Deck et al., 2004; Nicolle et al., 2004; Kleiven, 2007) and in ballistic impact studies with helmets. The intracranial pressures and relative brain–skull displacements in the aforementioned FEMs have been exercised and compared to either the intracranial pressures in Post mortem human subjects (PMHS) (Nahum and Smith, 1968; Trosseille et al., 1992), or to the relative brain–skull displacements from neutral density targets in PMHS (Hardy et al., 2001). However, the existing comparisons are typically incomplete, due to modeling approximations in loading, material properties, and specimen geometry and these evaluations are for blunt impact or inertial responses.

Therefore, the purpose of this study was to develop a high fidelity human head finite element model (HHFEM) that would be identical to a human surrogate head model (HSHM) in both size and in the level of anatomical detail. These paired models allow a one-to-one comparison of intracranial pressures and relative brain–skull displacements when the models are subjected to either shock tube or primary blast overpressures. In order to better understand the short term kinetic and longer term kinematic effects on the human brain; this model is attached to a FEM simulating the Hybrid III Anthropometric Test Device neck. A computational fluid dynamics (CFD) model of the head was developed and validated with experimental shock tube studies. This CFD model was then used to produce both the temporal and spatial pressure profiles equivalent to those seen on the HSHM and applied to the HHFEM. The HHFEM relative brain–skull displacements, intracranial pressures and global head rotations have been compared with those in the HSHM experimental shock tube tests.

2. Human surrogate head model (HSHM)

The process of fabricating the HSHM starts with using solid model files of the HHFEM in the formation of rapid prototype (RP) parts (two halves of the skull, the neck mount and the facial features), followed by the creation of silicon rubber molds of each part of the head and ending with the molding and assembly of the skull, brain and face. The skull was fabricated using a glass/epoxy material and the brain was created using the Sylgard gel. The RP

* Corresponding author. Tel.: +1 443 778 3788; fax: +1 443 778 6914.
E-mail address: jack.roberts@jhuapl.edu (J.C. Roberts).

0021-9290/$ - see front matter © 2012 Elsevier Ltd. All rights reserved.
http://dx.doi.org/10.1016/j.jbiomech.2012.07.027

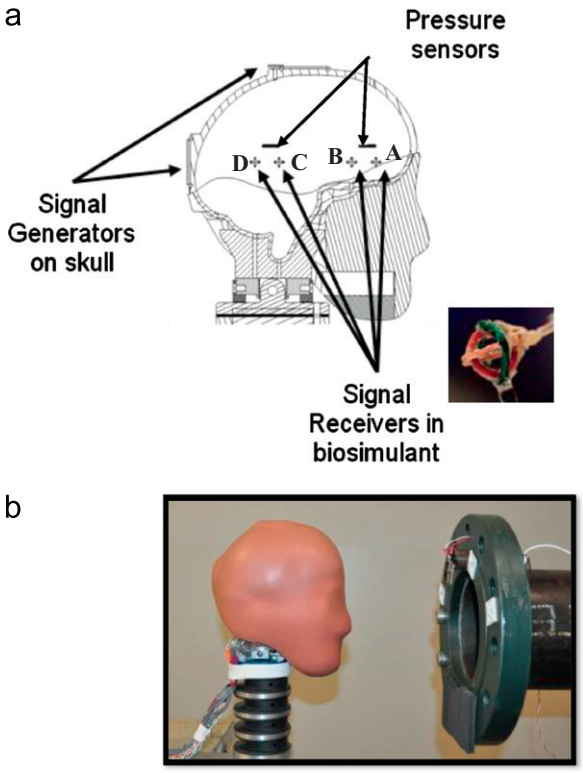

Fig. 1. (a) EMF displacement and pressure sensor locations in the HSHM; (b) completed HSHM in front of shock tube.

parts were then used to produce silicone rubber molds in order to fabricate the epoxy glass components of the skull. Six degree of freedom Electromotive Force (EMF) displacement sensors and pressure sensors were molded into the Sylgard brain material. The custom displacement sensors were comprised of three (3) transmitters orthogonally located on the surface of the skull and four (4) 5 mm diameter receivers embedded in the saggital section of the brain biosimulant. These sensors measure the displacements and rotations in all three orthogonal directions, i.e., x, y and z. Two of the displacement sensors are in the frontal region (locations A and B), approximately 5 mm apart, and two are in the parietal region (locations C and D), again 5 mm apart (Fig. 1a). There were also two (2) piezoresistive pressure sensors placed between the two pairs of generators. The neck mount, Hybrid III neck and facial features were then attached to the skull and all these components were encased in the skin. The HSHM was then placed in front of a shock tube and tests were performed at 517, 690 and 861 kPa shock tube driver pressures (Fig. 1b). A list of component parts, materials and manufacturers is shown in Table 1. A description of the creation, assembly and testing of the HSHM with and without a helmet is given in Merkle et al. (2010) and detailed results will be published in a comparison paper.

3. Computational model development

A finite element model of the human head created with LS-DYNA was obtained from the Volpe National Transportation Research Center[1] (Dimasi et al., 1991). The model was modified by the addition of the Livermore Software Technology Corporation (LSTC) Hybrid III Anthropometric Test Device (ATD) neck FEM. This required the addition of a head/neck interface occipital joint to create the final human head finite element model (HHFEM). Solid model files of the HHFEM were used to create the HSHM. The final HHFEM consisted of the face, skull, brain, brain stem and Hybrid III neck and contained 130,000 hexahedral, tetrahedral, shell and beam elements. The material used for brain tissue in the HSHM was silicone gel brain simulant Sylgard 527. Based on the interaction of this brain simulant with the inside of the HSHM skull, the boundary conditions between brain and skull in the HHFEM were modeled as tied contact surfaces. The coordinates in the head model consisted of the following: the positive x-axis is Anterior–Posterior ($+x$ toward nose), y-axis is Medial–Lateral ($+y$ toward right ear) and the z-axis in the Superior–Inferior ($+z$ toward neck) (Fig. 2). The Kelvin–Maxwell viscoelastic model was chosen for brain tissue to minimize parameters while capturing the essential mechanical behavior of the tissue, and while retaining a physical understanding of the parameters used. Material Properties for the non-brain structural components of the surrogate model were taken from testing and literature values. The material properties used for all parts in the HHFEM, which correspond to the actual material properties in the HSHM are shown in Table 2. To investigate high-frequency components of pressure predictions, the skull material was also evaluated as viscoelastic with properties shown in Table 2. Dynamic relaxation was used to arrive at the initial condition for the Hybrid-III neck; this included pre-compression of the slits in the rubber neck parts.

In order to model the overpressures that result from testing the HSHM in front of a shock tube, a CFD model of the head-form in front of a shock tube was required. The CFD software VULCAN was utilized to conduct this analysis. A surface grid of the head model was imbedded in a structured half-symmetry grid at the exit of the shock-tube system to mimic the experimental set-up for the HSHM (Fig. 3a). The shock structure developing out of the tube then impacts the surface of the face (Fig. 3b). This figure also shows a 2-D slice on the symmetry plane of only a portion of the domain as well as a side view of the 3-D surface of the head (Fig. 3c). These pressure data outputs from the CFD model were then exported for use as pressure inputs for the HHFEM. These CFD pressures for 517, 690 and 862 kPa are shown in Fig. 4.

4. Results

The HSHM measurements of intracranial pressure (ICP), relative brain-to-skull displacement (RBSD), and relative rotation

Table 1
Components, materials and manufacturers for parts in the HSHM.

Component	Material	Manufacturer
Facial structure	XP-656	Silicones Inc.
Neck mount	EPON 862+EPIKURE 3274+EPIKURE 3234+Synatactic foam VF-32	Miller–Stephenson and Fiber Glast Development Corp.
Skull	EPON 815C+EPIKURE 3234+KEN-REACT KZ 55 + # 29–1/16-inch milled glass fiber	Miller–Stephenson and Fiber Glast Development Corp.
Brain	Sylgard 527	Dow Corning
Skin	XP-656	Silicones Inc.
Piezo-resistive pressure sensors	Part no. EPIH-412-3000P/LAF	Measurement Specialties Inc.
EMF displacement sensors	Non-provisional patent application entitled "Methods and Systems to Implement a Surrogate Head Model and Directly Measure Brain/Skull Relative Displacement", Roberts, J.C., Merkle, A.C., Carkhuff, B.G., Wing, I.D., Leese, C.B., Serial no. 13/168,490, filed 6/28/11	

[1] National Crash Analysis Center at George Washington University, http://www.ncac.gwu.edu/

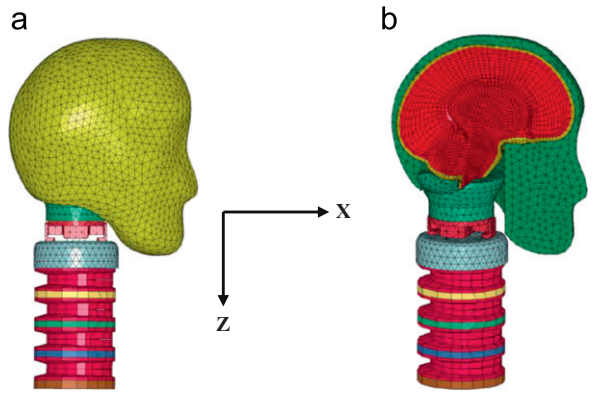

Fig. 2. Completed HHFEM and (b) saggital plane slice through the head.

Table 2
Parts, materials types and material constants for the HHFEM.

Part	Material type	Material's constants
Skull	Elastic	E=8.0 GPa, v=0.22, ρ=2.08 g/cc
Skull	Viscoelastic	K=2.38 GPa, G_0=1.64 GPa, G_∞=1.025 GPa, β=2.0/msec, ρ=2.08 g/cc
Brain	Viscoelastic	K=1.07 GPa, G_0=1.2 KPa, G_∞=0.25 kPa, β=0.08/msec, ρ=0.97 g/cc
Hybrid II neck rubber	Viscoelastic	K=112 MPa, G_0=2.3 MPa, G_∞=0.5 MPa, β=0.09/msec, ρ=1.1 g/cc
Face foam	Elastic	E=300 MPa, v=0.49, ρ=0.361 g/cc
Skin	Elastic	E=10 MPa, v=0.40, ρ=1.1 g/cc
Neck nod part	Elastic	E=70 GPa, v=0.33, ρ=2.7 g/cc
Head/neck interface	Elastic	E=13 GPa, v=0.33, ρ=1.1 g/cc
Top neck disc	Elastic	E=70 GPa, v=0.33, ρ=2.7 g/cc
Upper bracket	Elastic	E=70 GPa, v=0.33, ρ=2.7 g/cc
Neck discs	Elastic	E=70 GPa, v=0.33, ρ=2.7 g/cc
Lower neck bracket	Elastic	E=70 GPa, v=0.33, ρ=2.7 g/cc
Inside cable	Elastic	E=10 MPa, v=0.30, ρ=1.0 g/cc

E=Elastic modulus, v=Poisson's ratio, ρ=Density, K=Bulk modulus, G_0=Short term shear modulus, G_∞=Long term shear modulus, β=Time constant.

between small regions of the brain and the skull were calculated by the HHFEM, to allow direct comparison between predicted and measured data. The intracranial temporal pressures predicted in the HHFEM were compared to the measured values in the HSHM at anterior location of the brain for simulated shock tube driver pressures of 517, 690 and 862 kPa (Fig. 5). Although these pressures plots are for the anterior portion of the brain, the ICP's in the HHFEM and HSHM have the same trend in the posterior portion of the brain. For a given shock tube overpressure (690 kPa), a viscoelastic material model of the skull (Fig. 5b) more closely approximates the overall pressure decay with time in the HSHM (Fig. 5d). The difference between the HHHFEM and HSHM peak ICP's for driver pressures of 517, 690 and 862, were less than 25%.

The relative brain–skull temporal displacements and rotations at locations B, C and D in the HSHM (Fig. 1) were compared to the calculated RBSD in the HHFEM (Figs. 6–8). The EMF sensor at position A in the HSHM was found to have mechanical problems and was omitted from this paper. The sign of the peak RBSD's calculated by the HHFEM was the same as that measured in the HSHM for most simulated driver pressures, in both the

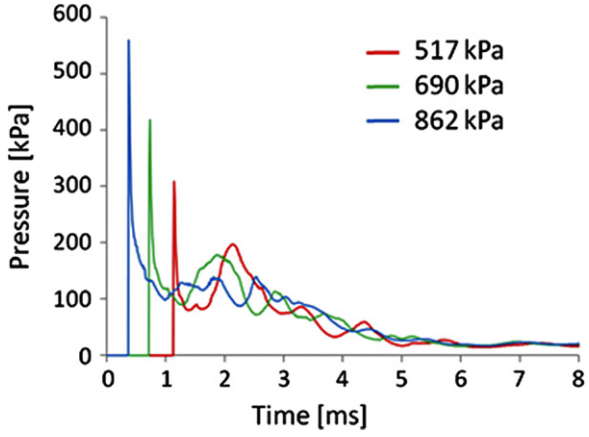

Fig. 4. CFD pressures on the head-form for shock tube driver pressures of 517, 690 and 862 kPa.

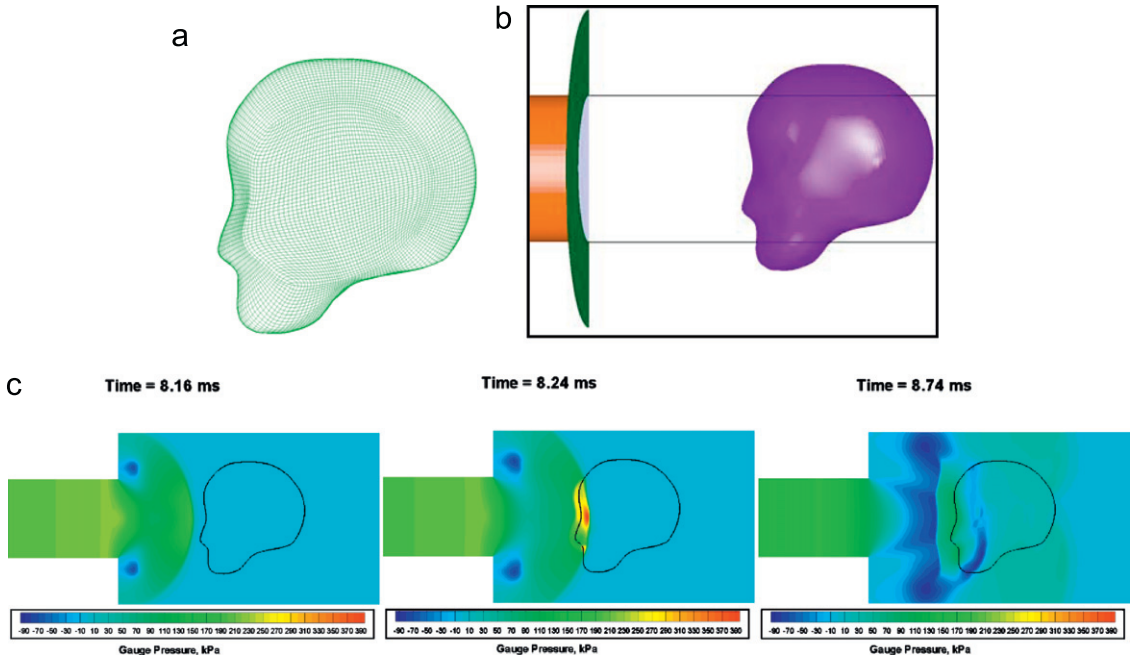

Fig. 3. (a) Surface grid and (b) CFD model of the head in front of the shock tube and (c) side view of a 2-D slice of the 3-D CFD model.

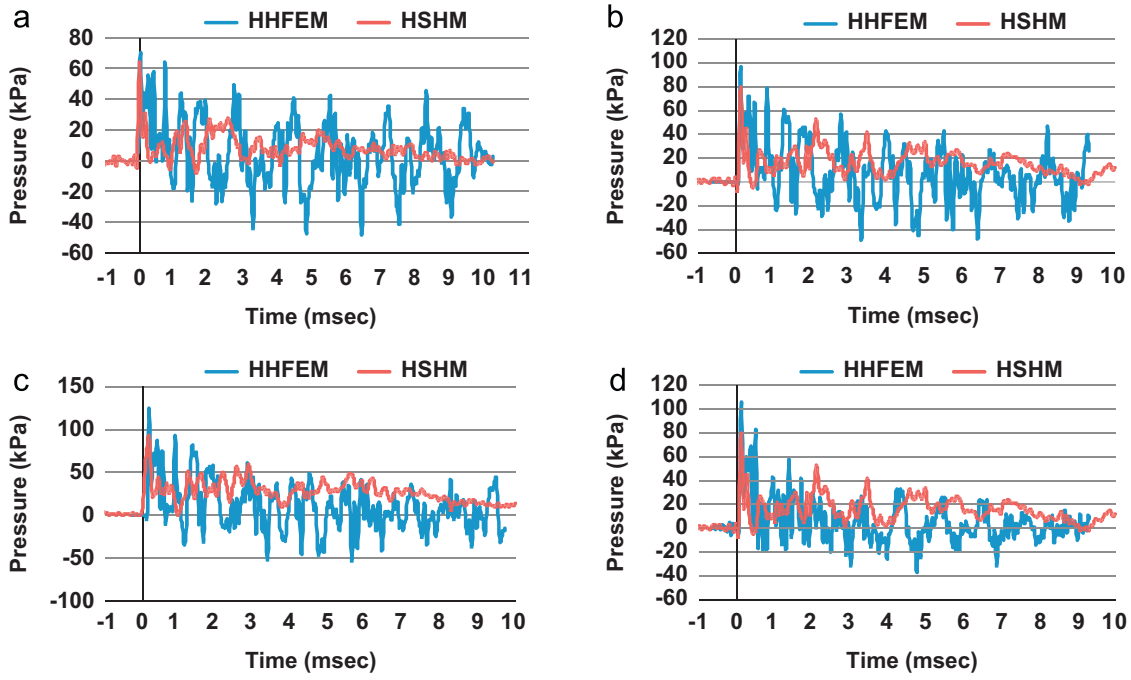

Fig. 5. Numerical and experimental intracranial pressures (ICP) for (a) 517, (b) 690 and (c) 862 kPa shock tube driver pressures in the anterior portion of the brain using an elastic skull model while (d) is the 690 kPa load case for a viscoelastic skull model.

anterior–posterior (AP) and superior–inferior (SI) directions, at sensor locations B and C. In general the trend is for the peak RBSD of the HHFEM and the HSHM to occur at the same time somewhere in the first 10–50 ms. Also, the temporal displacements plots of the HHFEM and HSHM damp out at about the same time and in about the same manner, and the HSHM RBSD peaks tend to occur somewhat before the HHFEM. The *x*-*z* RBSD in the saggital plane for the EMF sensors in the HSHM were compared to those in the saggital plane from the HHFEM for shock tube drive pressures of 517, 690 and 862 kPa (Figs. 6–8). For positions B and D, the HHFEM and HSHM paths were the same both in spatial directions, i.e., AP and SI, and in absolute values. At position C, there was a greater divergence in the paths with the HHFEM looking the same as at locations B and D and the HSHM exhibiting a more circular spatial orientation.

Rotation of the EMF displacement sensors at positions B, C and D in the HSHM was compared to calculated rotations from the HHFEM at shock tube driver pressures of 517, 690 and 862 kPa (Figs. 6–8). Since the pressure wave is coming from the AP direction and the rotations are measured in the mid-plane of the skull, the material around the sensor will primarily rotate about the medial–lateral axis. Unlike the RBSD's, the peak rotations of sensors in the HSHM occurred at about the same time and were of the same sign as the finite element calculations in the HHFEM at all shock tube driver pressures.

5. Discussion

The temporal ICP plots for an elastic skull material model (Fig. 5) show good agreement with peak pressures for all driver pressures, and show an influence of skull viscoelasticity on pressure histories. As can be seen in Fig. 4 the peak applied pressures on the HHFEM that resulted from the three simulated driver pressures were about 300, 420 and 560 kPa over a 2 ms time period. This pressure range was selected to approximate live-fire conditions that are known to cause a low probability of lung injury (Bowen et al., 1968). The peak ICP's agreed fairly well; the maximum differences between the HHFEM and HSHM were about 25%. These figures also indicate that the HHFEM pressures, on the whole, are under-damped compared to the experimental data for an elastic skull. When the elastic material model for the skull was changed to a viscoelastic material model (seen in Fig. 5(d) for a driver pressure of 690 kPa), these pressure oscillations decreased significantly. It was discovered that there were flexural waves that had developed in the elastic skull, which had caused continued ringing and under-damping in the ICP temporal plots. Therefore, it would be appropriate to consider the skull as a viscoelastic material when dealing with multi-frequency load applications.

The peak relative RBSD's (Figs. 6–8) show that as the shock tube driver pressures increase, the RBSD increase for all locations in the HHFEM. Also, a complete description of brain motion can be seen when combining the temporal displacements (Figs. 6–8(a) and (b)) with the spatial displacements (Figs. 6–8c). For instance, the peak RBSD in the *x*- and *z*-directions in the anterior portion of the brain at locations B (Fig. 6(a) and (b)) are in the negative *x*-direction and positive *z*-direction, which when combined with spatial plots (Fig. 6c) clearly indicates that the brain is initially moving in the posterior-superior directions. The peak RBSD's at location C (Fig. 7(a) and (b)) tend to be in the (slight) positive *x*- and *z*-directions, which indicates that the brain in the posterior location of the head hit by the pressure wave, is initially moving in the anterior-inferior direction, and again is verified by the RBSD plots in Fig. 7(c). Combining the results at locations B and C would indicate that in the first 20 ms the brain is rotating in a clockwise direction relative to the skull, which indicates that the shock wave not only imparts a compression wave to the brain but also induces a shearing wave. The direction that the HHFEM predicts for peak RBSD depends on the location of the points selected to record the RBSD with respect to the center of rotation of the head, which is different from rotation of the head on the neck.

The rotational head motion allowed by the neck (Hybrid-III) will result in larger RBSD than in head models with no neck. This is clearly seen by looking at the RBSD at locations C and D.

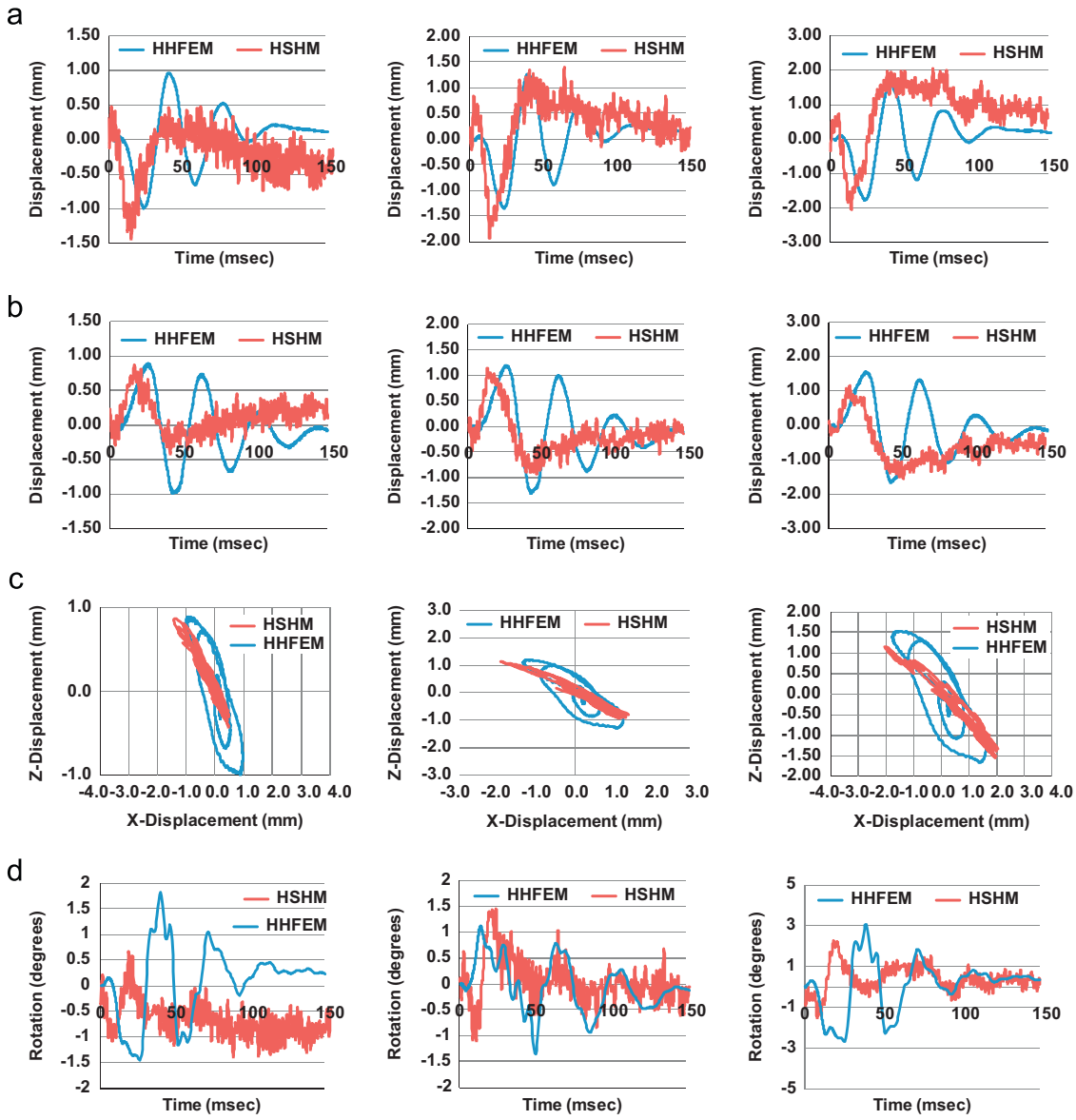

Fig. 6. A comparison of HHFEM and HSHM RBSD and rotations at sensor B (Fig. 1) for shock tube driver pressures of 517, 690 and 862 kPa, reading left to right. (a) *x*-direction temporal, (b) *z*-direction temporal, (c) *x*–*z* spatial and (d) rotations.

The RBSD's at position D, being farther from the center of rotation of the head–neck system is between 2 and 3 times greater than that at position C. The peak RSBD's at position D in Fig. 8 are almost entirely in the superior direction with very little anterior–posterior component to the brain motion. These predicted and validated motions for points within the brain show the type of brain movement that corresponds to large areas of induced strain. For individuals exposed to a blast due to an IED, there could be diffuse axonal injury (DAI) due high head accelerations over longer period of time.

As with any finite element model, there are differences due to the effects of material models, material properties and boundary conditions. A linear constitutive model was used for brain tissue, but geometric nonlinearities (due to rotation) were accounted for in LS-Dyna, so the analysis is not linear. The peak principal strain values were less than 15%, which indicates that the model chosen for the silicone gel brain simulant is adequate for the loading situations. In the physical model (HSHM), the silicone gel that mimics brain material is adhesive to the skull and is well-stuck to the inside of the skull, being poured into place. In the HHFEM, the tied contact interface does not allow failure. Checks on pressures show this to be appropriate, since the absolute pressure at these interfaces was always positive. For separation at the interface, a net tension is necessary, and since the shear modulus of the brain surrogate is a very small fraction of the bulk modulus, this means that a negative absolute pressure is necessary. We did not find that in any of our calculations. Also, these boundary conditions are more in line with other human head finite element models in the literature, i.e., Kleiven (2003), Horgana and Gilchrist (2004), Zhang et al. (2001), and Kleiven and Hardy (2002).

The percent differences in RBSD's between the HHFEM and HSHM at positions B, C and D are shown in Table 3. At positions B and D the differences between the peak RBSD in the HSHM and the HHFEM are between 5% and 41%, which is very reasonable for a very complex model with material properties that are strain rate dependent and boundary conditions that must be approximated in order to make the computations. The displacement profiles in the HSHM (not shown) indicated a substantial gradient in displacements near the location of displacement transducer C, indicating that the brain simulant in that region was rotating

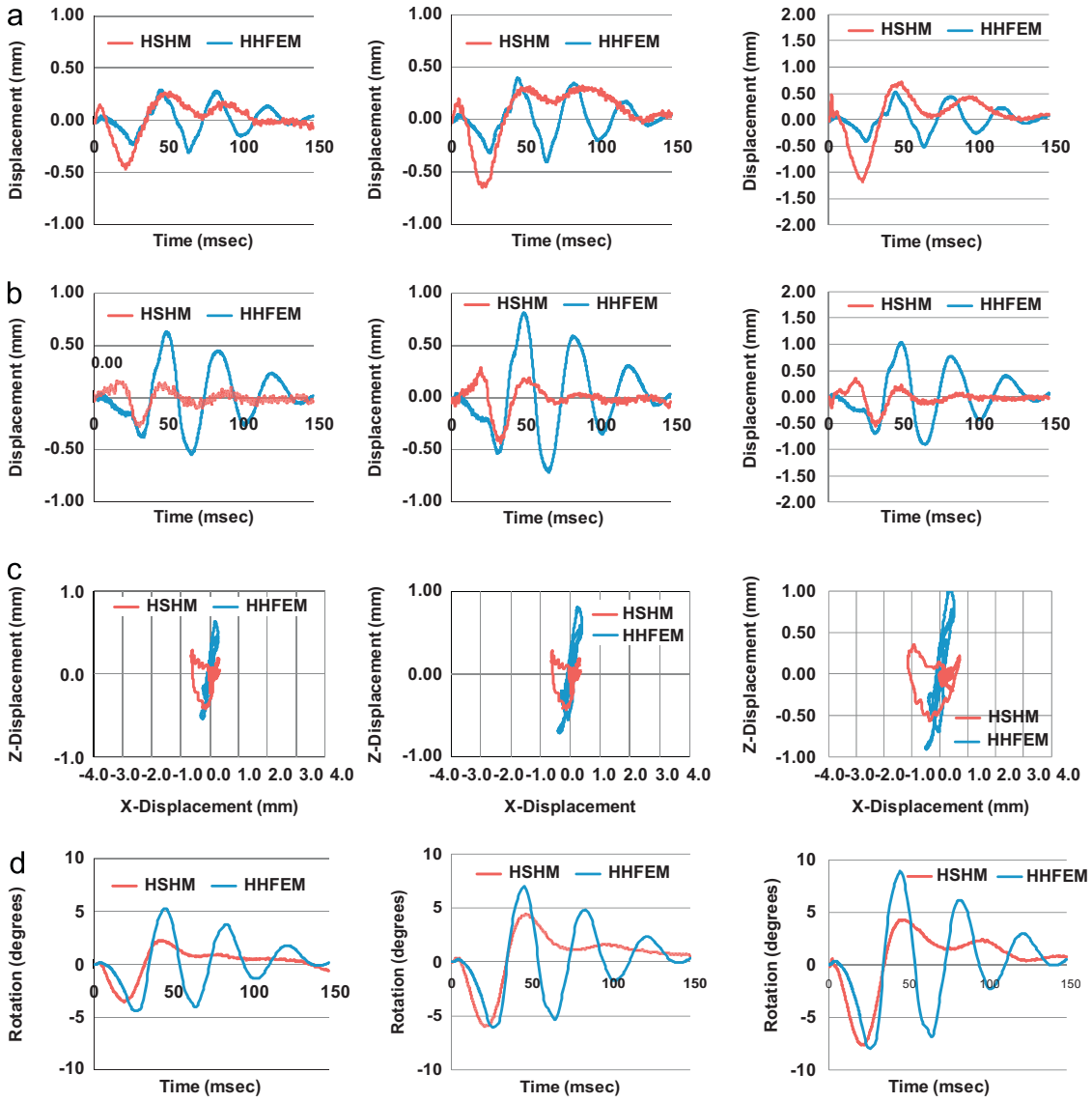

Fig. 7. A comparison of HHFEM and HSHM RBSD and rotations at sensor C (Fig. 1) for shock tube driver pressures of 517, 690 and 862 kPa, reading left to right. (a) *x*-direction, (b) *z*-direction, (c) *x*–*z* spatial and (d) rotations.

relative to the skull. This made displacement predictions from the finite element mesh difficult, since small changes in the location used for the predicted displacement caused changes in magnitude and sometimes sign. The locations used were based on the plans for the surrogate, but the as-built locations may have been slightly different, leading to the greater discrepancies (~60%) seen in RBSD's at location C. Also, even though the sign of the displacements of the HSHM and the HHFEM at location D in the model are reversed, the absolute value of the peak magnitudes of the RBSD's differ by, at most, 26%.

The differences in RBSD's when comparing human head finite element results to PMHS blunt impact tests with different material models for the brain were comparable to the differences seen in the present study using a surrogate head model with brain simulant properties. The model by Zhang et al. (2001) in using human brain tissue properties for the short term, long term and decay constant for the linear viscoelastic model, resulted in brain displacements that were up to 60% different when comparing the finite element model to blunt impact tests on PMHS, Hardy et al. (1997). Also, in Kleiven and Hardy (2002) whether a hyperelastic or linear viscoelastic material model was used for brain tissue and regardless of whether the brain properties were "compliant", "average", or "stiff", the peak displacements in the brain of the finite element model were between 5% and 100% different from those that were measured in the same blunt impact PMHS experiments as in Hardy et al. (1997). Again, in the finite element head model developed in Deck et al. (2004), when using a hyperelastic or linear viscoelastic material model for the brain, the relative brain–skull displacements from the model were anywhere from 5% to 75% different that those displacements measured in blunt impact test on PMHS, Hardy et al. (1997).

It is very difficult to directly compare the results of relative brain–skull displacements from this study with others, because to date other studies have only considered high head accelerations or blunt impact to the heads of PMHS when looking at displacement measurements. The peak displacements in Table 3 range from about 0.3–3 mm in both directions in the anterior and posterior portions of the brain. Zhang et al. (2001), Kleiven and Hardy (2002), Horgan and Gilchrist (2004), Deck et al. (2004) and Takhounts et al. (2003) used head FEM's to compare to the experimental data from Nahum et al. (1977), Trosseille et al. (1992) and Hardy et al. (1997). The resulting ICP ranged from

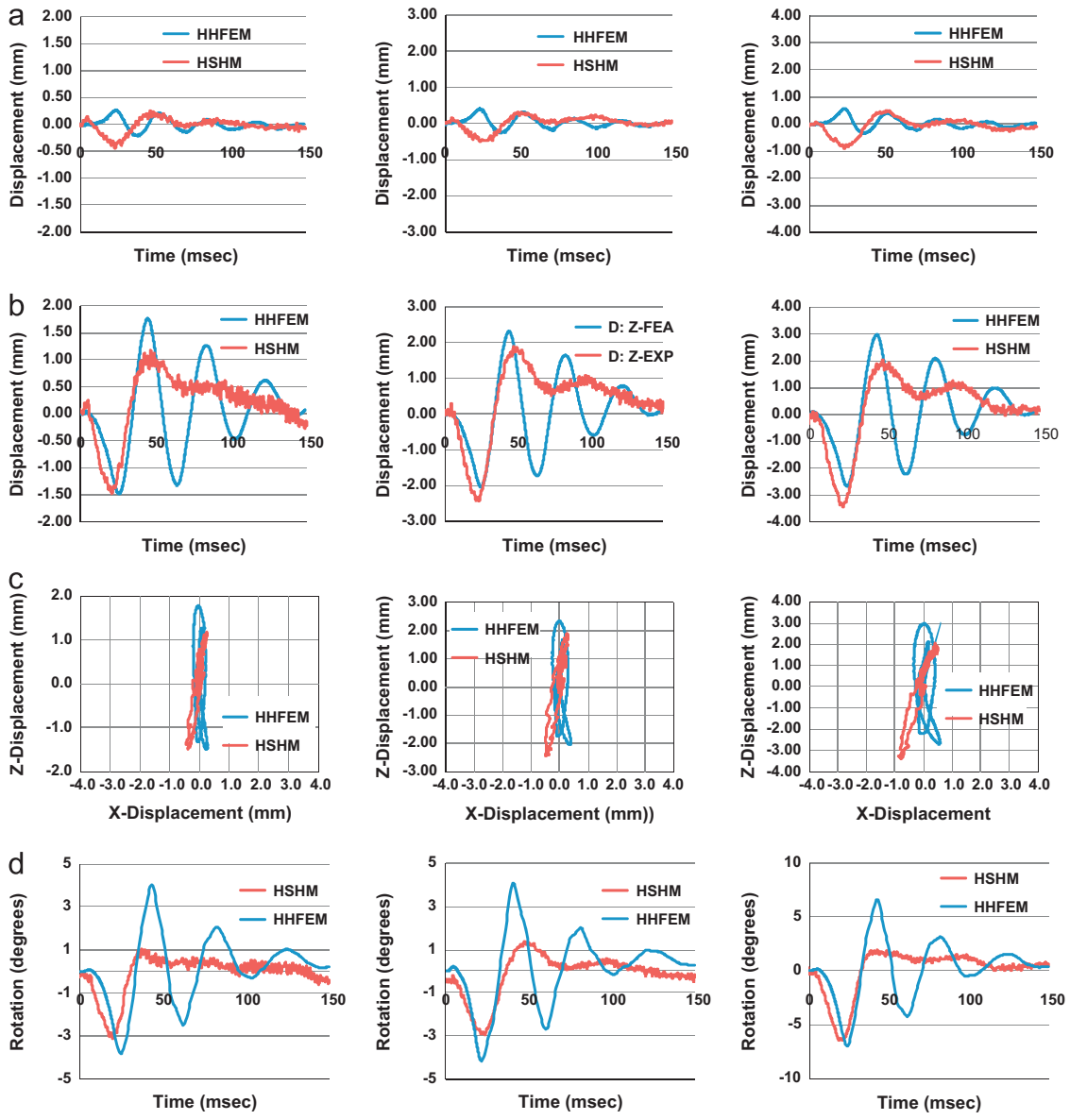

Fig. 8. A comparison of HHFEM and HSHM RBSD and rotations at sensor D (Fig. 1) for shock tube driver pressures of 517, 690 and 862 kPa, reading left to right. (a) *x*-direction, (b) *z*-direction, (c) *x*–*z* spatial and (d) rotations.

Table 3
Differences in the HHFEM and the HSHM peak relative brain–skull displacements (RBSD) at different sensor locations (in Fig. 1).

Shock tube Driver Pressure (kPa)	HHFEM X-Direction (mm)	HSHM X-Direction (mm)	% Difference[a]	HHFEM Z-Direction (mm)	HSHM Z-Direction (mm)	% Difference[a]
	Position B					
517	1.62	1.15	**29**	1.11	0.71	**36**
690	2.22	1.86	**16**	1.48	0.868	**41**
862	3.00	2.00	**33**	1.91	1.21	**37**
	Position C					
517	0.272	0.540	**50**	0.576	0.213	**60**
690	0.435	0.584	**25**	1.00	0.32	**68**
862	0.490	1.14	**57**	1.20	0.490	**60**
	Position D					
517	0.372	0.390	**5**	1.72	1.27	**26**
690	0.523	0.490	**6**	2.44	2.19	**10**
862	0.694	0.800	**13**	3.00	3.10	**3**

[a] % Difference = Max − Min/Max.

80–150 kPa and the displacements ranged from 2–6 mm for blunt impact loads to the model. As previously mentioned, the overpressure loads in the current study are considered sub-lethal and therefore, it is not surprising that the ICP's and RBSD's are much lower than in the blunt impact load cases. There was comparable agreement between the numerical with experimental peak ICP results in these papers as in the current study, i.e., less than 25% difference. In a more recent study by Sharma and Zhang (2011), using the Wayne State human head finite element model exercised with a blast peak pressure of 460 kPa over a 1.5 ms time period, the resulting peak ICP in the frontal portion of the brain was about 100 kPa. When the HHFEM in the current study was exercised with a peak pressure of 300 kPa over about a 1.2 ms time period the resulting peak ICP in the anterior portion of the brain was 70 kPa. Although the exact location that the pressures are taken from are not known, material properties used in the two models are different (HHFEM uses Sylgard properties and the Wayne State model uses human brain properties) and the head geometry is different, this comparison still shows that as the peak pressures and duration (impulse) decrease, the peak ICP decreases as would be expected. Also, the spatial x–z plots of RBSD seen in Figs. 6–8 are very similar to those seen in the experimental work shown in Hardy et al. (1997).

A finite element model (FEM) of a human head attached to a Hybrid III ATD neck has been developed and validated against an identical human surrogate head model in shock tube tests. In order to translate the applied pressure loads to the head FEM, a CFD model of the head was developed and exercised for simulated driver pressures in the experimental tests of 517, 690 and 862 kPa. Intracranial pressures and displacements from sensors in the surrogate head model were compared to those seen at the same locations in the finite element model. Peak intracranial pressures seen in the head FEM were within 25% of those seen in the surrogate head model, while peak relative brain–skull displacements in the head FEM, in most locations, were within about 30–40% of those seen in the human surrogate head model. This head model will be further enhanced with addition of a falx, tentorium and CSF, as well as, realistic human neck and compared to Post Mortem Human Subject (PMHS) in future shock tube tests.

Conflict of interest statement

None declared.

Acknowledgments

The authors would like to express their appreciation to the Office of Naval Research (ONR) and the Department of Defense Congressionally Directed Medical Research Programs (CDMRP) under contracts N0001407PD20006 and W81XVVH-09-2-0168, respectively, for supporting this work. The content included in this work does not necessarily reflect the position or policy of the US Government.

References

Bowen, I.G., Fletcher, E.R., Richmond, D.R., 1968. Estimate of Man's Tolerance to the Direct Effects of Air Blast, Technical Progress Report, Technical Progress Report, DASA-2113. Defense Atomic Support Agency, Department of Defense, Washington, DC.

Brands D.W.A., 2002. Predicting Brain Mechanics During Closed Head Impact. Ph.D. Thesis. Technische Universiteit Eindhoven, The Netherlands.

Claessens M., Sauren, F., Wisemans, J., 1997. Modeling of the human head under impact conditions: a parametric study. In: Proceedings of the 41st Stapp Car Crash Conference, Society of Automotive Engineers, Warrendale, PA, pp. 315–328.

Deck C., Nicolle, S., Willinger, R., 2004. Human head FE modeling: improvement of skull geometry and brain constitutive laws. In: Proceedings of the IRCOBI Conference, Graz, Austria, pp. 79–82.

Dimasi F., Marcus, J., Eppinger, R.H., 1991. 3-D (three-Dimensional) anatomic brain model for relating cortical strains to automobile crash loading. In: Proceedings of the 13th International Technical Conference on Experimental Safety Vehicles, Nov 4–7, 1991, Paris, France, pp. 2.

Hardy W.N., Foster, C.D., King, A.I., Tashman, S., 1997. Investigation of brain injury kinematics: introduction of a new technique. AMD-vol 225/BED-vol 38, Crashworthiness, Occupant Protection and Biomechanics in Transportation Systems.

Hardy, W.N., Foster, C.D., Mason, M.J., Yang, K.H., King, A.I., 2001. Investigation of head injury mechanisms using neutral density technology and high speed biplanar X-ray. Stapp Car Crash Journal 45, 337–368.

Horgan, T.J., Gilchrist, M.D., 2003. The creation of a three dimensional finite element model for simulating head impact biomechanics. International Journal of Crashworthiness 8 (4), 353–366.

Horgan, T.J., Gilchrist, M.D., 2004. Influence of FE model variability in predicting brian motion and intracranial pressure changes in head impact simulations. International Journal of Crashworthiness 9 (4), 107–133.

Kang H.-S., Willinger, R., Diaw, B.M., Chinn, B., 1997. Validation of a 3-D anatomic human head model and replication of head impact in motorcycle Accident by Finite Element Modeling. In: Proceedings of the 41st Stapp Car Crash Conference, Lake Buena Vista, Florida, pp. 329–338.

Kleiven S., 2002. Finite Element Modeling of the Human Head. Ph.D. Thesis. Department of Aeronautics, Royal Institute of Technology, Stockholm, Sweden.

Kleiven, S., 2003. Influence of impact direction on the human head in prediction of subdural hematoma. Journal of Neurotrauma 20 (4), 365–379.

Kleiven, S., 2007. Predictors for traumatic brain injuries evaluated through accident reconstructions. Stapp Car Crash Journal 51, 81–114.

Kleiven, S., Hardy, W.N., 2002. Correlation of an FE model of the human head with local brain motion-consequences for injury prediction. Stapp Car Crash Journal 46, 123–144.

Merkle, A.C., Wing, I.D., Roberts, J.C., 2010. Human surrogate head response to dynamic overpressure loading in protected and unprotected conditions. IFMBE Proceedings 32, 20–25.

Nahum A.M., Smith, R., Ward, C.C., 1977. Intracranial pressure dynamics during head impact. In: Proceedings of the 21st Stapp Car Crash Conference, Paper no. 770922, Society of Automotive Engineers.

Nahum A.M., Smith, R.W., 1968. An experimental model for closed head impact injury. In: Proceedings of the 12th Stapp Car Crash Conference, pp. 783–814.

Nicolle, S., Lounis, M., Willinger, R., 2004. Shear properties of brain tissue over a frequency range relevant for automotive impact situations: new experimental results. Stapp Car Crash Journal 48, 1–20.

Ruan, J.S., Khalil, T., King, A.I., 1993. Finite element modeling of direct head impact. In: Proceedings of the 37th Stapp Car Crash Conference, San Antonio, California, pp. 69–81.

Sharma S., Zhang, L., 2011. Prediction of intracranial responses from blast induced neurotrauma using a validated finite element model of the human head. In: Proceedings of the Ohio State University Injury Biomechanics Symposium, Columbus, Ohio, pp. 1–17.

Takhounts, E.G., Eppinger, E.H., J.Q., Campbell, Tannous, R.E., Power, E.D., Shook, L.S., 2003. On the development of the SIMon finite element head model. Stapp car crash journal 47, 107–133.

Trosseille, X., Tarriere, C., Lavaste, F., Guillon, F., Domont, A., 1992. Development of a FEM of the human head according to a specific test protocol. Stapp Car Crash Journal 36, 235–253.

Willinger, R., Baumgartner, D., 2003. Numerical and physical modeling of the human head under impact-towards a new injury criteria. International Journal of Vehicle Design 32 (1/2), 94–115.

Zhang, L., Yang, K.H., Dwarampudi, R., Omori, K., T, L., Chang, K., Hardy, W.N., Khalil, T.B., King, A.I., 2001. Recent advances in brain injury research: a new human head model development and validation. Stapp Car Crash Journal 45, 369–394.